Published by: ***Higher Institute of Engineering and Technology, Kafrelsheikh*** **(KFS-HIET)**

Journal homepage: https://jiet.journals.ekb.eg/

Print ISSN 3009-7207 **Online ISSN** 3009-7568

FE Analysis of Hexagonal High Strength Concrete-Filled Double-Skin Steel Tubular Short Columns Subjected to Axial Compressive Forces

Hend R. Selima

Civil Engineering Department, Higher Institute of Engineering and Technology, Kafrelsheikh, Egypt

Received: 18 January 2024; Revised: 24 March 2024; Accepted: 1 April 2024

ABSTRACT: Concrete-filled tubular double skin (CFDST) columns comprise a tube-in-tube configuration with concrete poured into the annular spaces between the hollow parts (such as natural compaction) or mortar. Aligning the double steel pipes creates space in the middle of the column, reducing the amount of concrete needed to construct the column. Currently, due in part to a lack of design standards, composite structures consisting of concrete-filled hexagonal double-layer tubular columns (HCFDST) with internal circular tubes have not been widely applied worldwide. The compression performance of these columns is investigated in this paper. Finite element analysis was used to determine the HCFDST columns structural characteristics. Using experimental data available for HCFDST, the suggested FEM model was validated to demonstrate the model correctness and dependability. A validated FE model was utilized to investigate the impact of various factors on the load-displacement response of short HCFDST columns through parametric studies conducted on the columns. This work proposes a novel formula to determine the ultimate load capacity of short HCFDST columns under axial compression.

KEYWORDS: Concrete-filled double skin tubular columns, high strength concrete, finite element simulation, ultimate bearing capacity, double layers, composite structure.

1. INTRODUCTION

Fundamental elements of the majority of structures are columns and as a result, precise column capacity prediction is essential to the structure's overall dependability and performance. There are many types of composite pillars with different cross-sections, However, encased I-section, concrete-filled steel tubes, and, more recently, double skin columns are the most widely utilized and studied varieties. Concrete is poured into steel tubes to make concrete-filled tubular steel (CFST) columns, and between two steel tubes to form concrete-filled double-layer tubular steel (CFDST) columns as shown in Fig. 1.

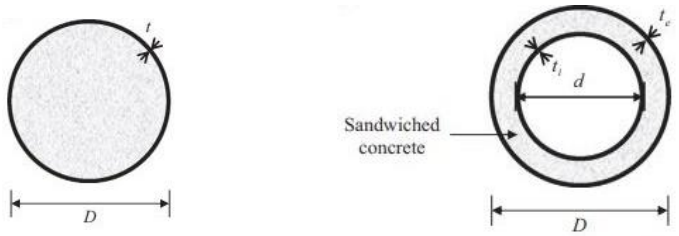

(a) CFST (b) CFDST

Fig. 1. Circular concrete-filled short column types: (a) CFST and (b) CFDST.

It was found that the application of CFDST columns shown in Fig. 2, reduced the constructions self-weight because of the hollow interior spaces [1-4]. It is well known that CFDST columns offer several advantageous characteristics, including excellent fire resistance, high strength, and bending stiffness [5] and seismic functionality [6–10]. CFDST has been utilized as piers for high-rise bridges that reduce the structure weight. [11]. The columns of CFDST have improved strength and ductility when compared with the conventional CFST columns [12-15].

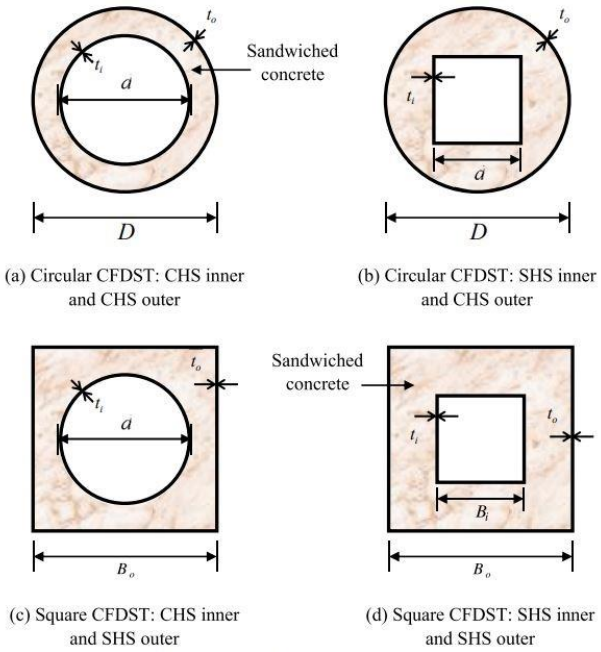

Fig. 2. CFDST column cross-section types: (a) Circular CFDST: CHS inner and CHS outer, (b) Circular CFDST: SHS inner and CHS outer, (c) Square CFDST: CHS inner and SHS outer, and (d) Square CFDST: SHS inner and SHS outer.

Hexagonal CFDST (HCFDST) members have been employed in the structure of tall buildings recently shown in Fig. 3. A total of thirty-six specimens are compressed while being operated under various conditions. Lastly, based on the filled concrete strength and the tubes' yielding strengths, equations were developed to calculate the compression strength of each.

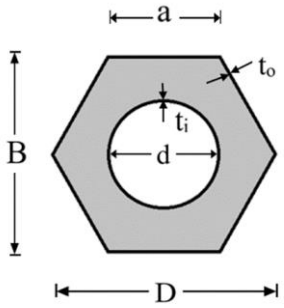

Fig. 3. Hexagonal CFDST: CHS inner and HHS outer.

2. FINITE ELEMENT MODELLING

2.1. General

The finite element program ABAQUS [16] is used to simulate and investigate the behavior of hexagonal short CFDST columns with inner circular tubes under compressive load. Boundary conditions, load application, element type selection, mesh size, and the interface between the steel tubes and concrete are all factors that affect the FE model.

2.2. Mesh and Type of Finite Element

The steel tubes and concrete in the HCFDST construction should be described using three-dimensional 8-Node solid elements (C3D8R) linear brick with decreased integration, linear geometric order, and hexahedron element shape [17]. The solid element (C3D8R) captures both the effective mesh at contact surfaces and the deflected shape of steel tubes [18–20]. The global mesh size of the steel tubes and the concrete infill, as determined by HCFDST, is approximately 20 mm as shown in Fig. 4.

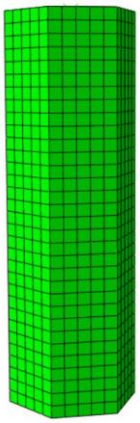

Fig. 4. Finite element mesh for CFDST columns.

2.3. Load Application and Boundary Conditions

Using the reference point (RF) of the top surface STATIC option in ABAQUS, the concentrated load was applied. As shown in Fig. 5., the axial displacement was permitted at the RF of the top surface in the direction of the applied load. The bottom surface of the columns' RF was blocked in all directions. The load was applied gradually using the adapted RIKS method from the ABAQUS library.

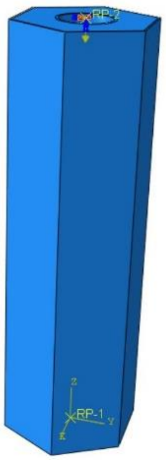

Fig. 5. Loading and boundary condition of the column.

2.4. Interactions

ABAQUS SURFACE INTERACTION option is used to create surface interaction attributes. The characteristics of the surface interface dictated contact interactions. The primary requirement was for the two faces to remain in touch with one another for the friction to persist. Surface-to-surface contact was selected to replicate the interaction between the steel tubes and concrete. Normal behavior defines "hard contact" as the interaction between two deformable surfaces in a normal direction. This permits tension separation following contact and keeps the surfaces from penetrating in compression. The friction coefficient (μ), which is assumed to be 0.3, specifies the contact surface tangential characteristics.

2.5. Material Modeling

2.5.1 Steel

To characterize the material model of the specimen, for steel, it is assumed that the elastic modulus (Es) and Poisson's ratio are 200 GPa and 0.3, respectively. Fig. 6. displayed the steel elastoplastic stress-strain curve [21].

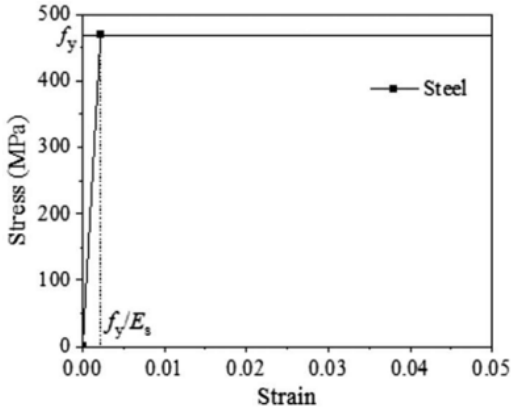

Fig. 6. Steel stress-strain curve.

2.5.2 Confined sandwich concrete material

The Drucker-Prager plasticity model simulates the behavior of concrete material under compression following the linear response, which is used to calculate the yield surface and the flow potential parameters for materials subjected to triaxial compressive pressures. The yield stage of restricted concrete is characterized by two parameters: DRUCKER PRAGER and DRUCKER PRAGER HARDENING. The linear Drucker-Prager model is used with related flow and isotropic requirements [22]. The stress vs. strain curves for confined and unconfined concrete in typical hexagonal CFST columns are shown in Fig. 7.

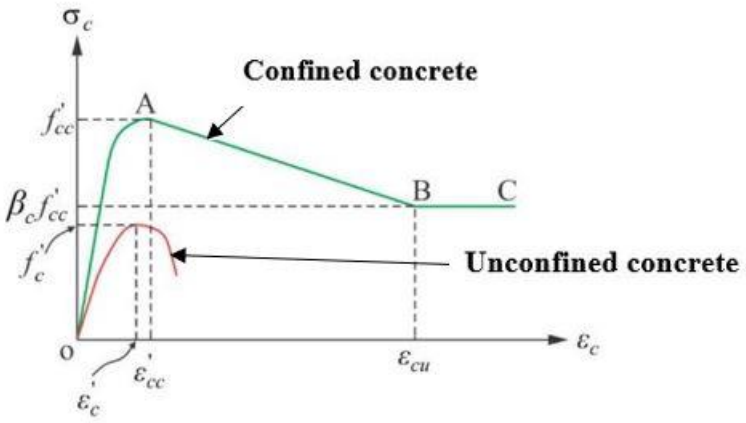

Fig. 7. Regular HCFDST stress-strain curve.

The part OA of the stress versus strain curve displayed in Fig. 7 is described by the formula illustrated in [23] and given in Eqs. (1) and (2) below.

$$\sigma_c = \frac{f'_{cc}\lambda\left(\frac{\varepsilon_c}{\varepsilon'_{cc}}\right)}{\lambda - 1 + \left(\frac{\varepsilon_c}{\varepsilon'_{cc}}\right)^{\lambda}} \quad (1)$$

$$\lambda = \frac{E_c}{E_c - \left(\frac{f'_{cc}}{\varepsilon'_{cc}}\right)} \quad (2)$$

where f'_{cc} indicates the confined concrete strength, ε'_{cc} is the strain at f'_{cc}, εc shows the concrete strain, σ_c represents the concrete stress at strain εc, and Ec defines the elastic modulus of concrete as provided in ACI 318-14 [24] and displayed in Eqs. (3) and (4) below.

$$E_c = 3320\sqrt{\gamma_c f'_c} + 6900 \text{ (MPa)} \quad (3)$$

$$\gamma_c = 1.85 D_c^{-0.135} \ (0.85 \le \gamma_c \le 1.0) \tag{4}$$

In this case, Dc is defined as (D - 2t), where t is the steel tube thickness and D is defined in Fig. 3. γc is the reduction factor for the effects of the column size effect. The formula in [23] is altered into [25], as indicated in the following Eqs. (5) and (6):

$$f'_{cc} = \gamma_c f'_c + 4.1 f_{rp} \tag{5}$$

$$\varepsilon'_{cc} = \varepsilon_c \left[1 + 20.5 \left(\frac{f_{rp}}{\gamma_c f'_c}\right)\right] \tag{6}$$

Where frp is the lateral confining pressure, ε'_c , is the unconfined concrete strain at f'_c , and f'_c is the concrete cylinder strength. A model for circular CFST columns under axial stress using numerical models is provided [25]. The following linear law that was put out to ascertain the regular hexagonal CFST's confinement pressure θ=120o is shown in Eq. (7):

$$f_{rp} = \begin{cases} \left(0.0491703 - 0.0007943 \dfrac{B+D}{2t}\right) f_{sy} & for\ 17 \le \dfrac{B+D}{2t} < 63 \\ \left(0.0065311 - 0.0000044 \dfrac{B+D}{2t}\right) f_{sy} & for\ 63 \le \dfrac{B+D}{2t} < 103 \end{cases} \tag{7}$$

Eq. (8) below provides the linear components AB and BC of the material law depicted in Fig. 7.

$$\sigma_c = \begin{cases} \dfrac{(f'_{cc} - \beta_c f'_{cc})(\varepsilon_{cu} - \varepsilon_c)}{(\varepsilon_{cu} - \varepsilon'_{cc})} + \beta_c f'_{cc} & for \quad \varepsilon'_{cc} < \varepsilon_c < \varepsilon_{cu} \\ \beta_c f'_{cc} & for \quad \varepsilon_c \le \varepsilon_{cu} \end{cases} \tag{8}$$

where εcu represents the strain in the concrete at Point B, and the value of εcu is equal 0.02 [26]. The factor that represents the confinement effects on strength and ductility in the post-peak range is called βc in Eq. (9). The value of βc is provided by:

$$\beta_c = 0.8726 - 0.006 f'_c \qquad for\ 47 \le \frac{B+D}{2t} < 103 \tag{9}$$

At $\beta_c < 47$, β_c is taken as 1.0 [26].

3. FE VALIDATION

The experimental results from investigation illustrated in [21] were used to assess the applicability of the FE modelling technique used here, as indicated in Table 1. The numerical to test ratios $N_{ul,F.E}$ / N_{Exp} and statistical factors related to this ratio, such as mean, standard deviation (SD), and coefficient of variation (COV), which are low values that indicated its dependability, are also included in Table 1.

Table 1: Ultimate bearing capacity of HCFDST columns.

Column	N_{Exp} Shen et al.[21]	$N_{ul\ FE}$	N_{FE} / N_{Exp}
H-L	3405.5	3490	**1.025**
H-L-P00	4160.7	3878	**0.932**
H-L-P30	3931.3	4085	**1.039**
H-L-P57	4145.3	4240	**1.023**
H-H	2975.3	3380	**1.136**
H-H-P00	3573.3	3779	**1.058**
H-H-P30	3855.5	3980	**1.032**
Mean			**1.035**
SD			**0.059**
COV			**0.058**

The load-axial displacement relationships for the columns, considering the experimental and FE responses, are depicted in Figs. 8.

4. PARAMETRIC STUDY

There were 12 numerical models generated in all. The findings are shown in Table 2. The specimens are named a A (D- d- fy- fc), where D and d are shown in Fig. 3, fc and fy are concrete strength and steel yield strength, respectively.

Table 2: Details and ultimate bearing capacity of the HCFDST columns FE models.

Outer tube dimensions			Inner tube dimensions			Hollow ratio	fy (Mpa)	fc (Mpa)	No	Nul,F.E (kN)
Do (mm)	to (mm)	Do/to	di (mm)	ti (mm)	di/ti	χ				
150	2	75	60	3	20	0.48	300	60	A150-60-300-60	1201
180	2	90	60	3	20	0.4	300	60	A180-60-300-60	1376
210	2	105	60	3	20	0.34	300	60	A 210-60-300-60	2157
150	2	75	50	5	10	0.4	300	60	A150-50-300-60	1316
150	2	75	70	5	14	0.56	300	60	A150-70-300-60	1297
150	2	75	85	5	17	0.68	300	60	A150-85-300-60	1252
150	2	75	60	3	20	0.48	300	70	A150-60-300-70	1314
150	2	75	60	3	20	0.48	300	80	A150-60-300-80	1425
150	2	75	60	3	20	0.48	300	90	A150-60-300-90	1536
150	2	75	60	3	20	0.48	240	60	A150-60-240-60	1115
150	2	75	60	3	20	0.48	350	60	A150-60-350-60	1271
150	2	75	60	3	20	0.48	450	60	A150-60-450-60	1406

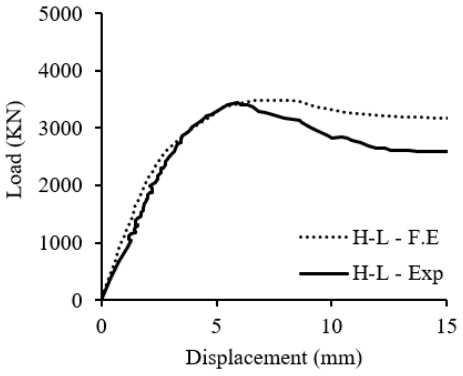

(a) H-L

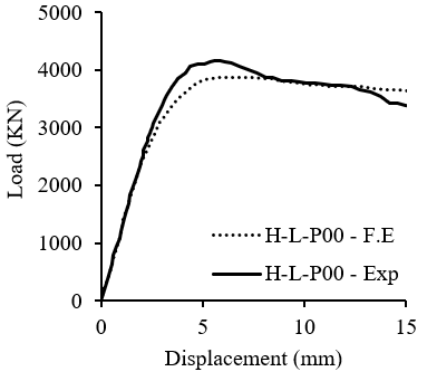

(b) H-L-P00

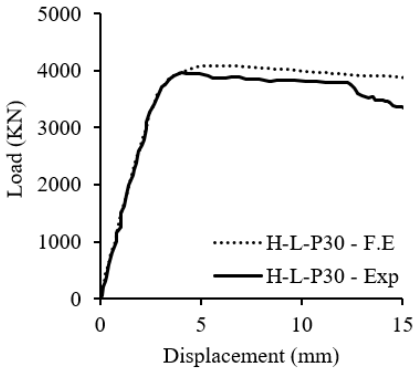

(c) H-L-P30

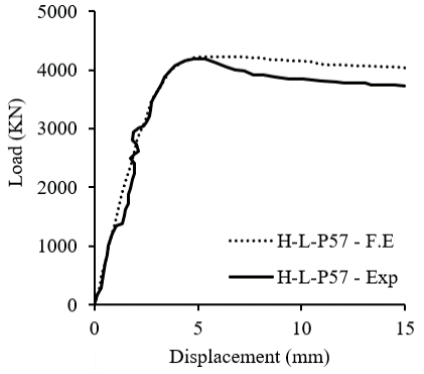

(d) H-L-P57

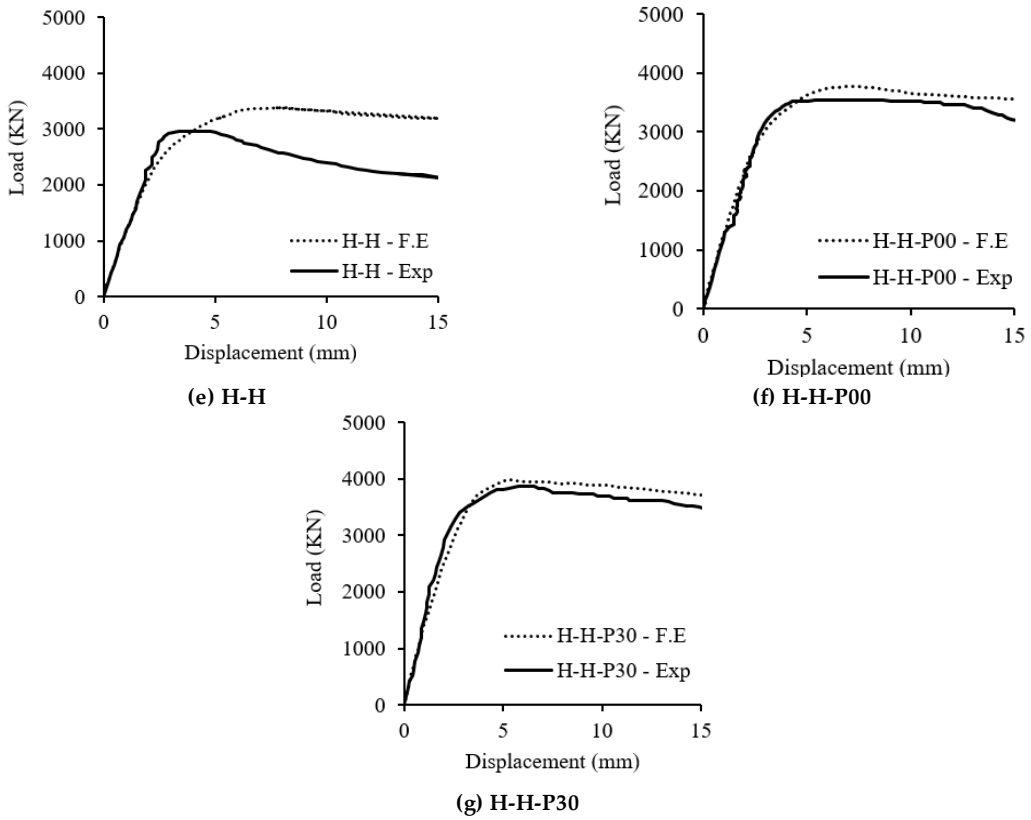

(e) H-H **(f) H-H-P00**

(g) H-H-P30

Fig. 8. Comparison of the load-displacement curves of specimens using FE modelling and experimental data: (a) H-L, (b) H-L-P00, (c) H-L-P30, (d) H-L-P57, (e) H-H, (f) H-H-P00, (g) H-H-P30.

4.1. Effect of Do/to

The HCFDST columns load- displacement curves with different Do/to ratios are displayed in Fig. 9.

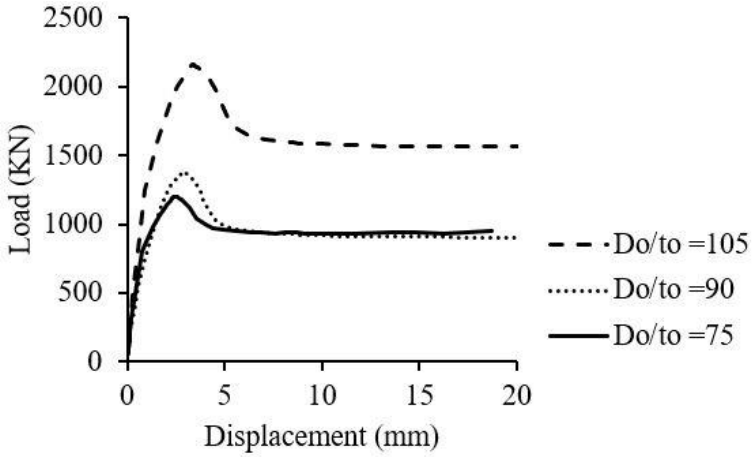

Fig. 9. Load–displacement curves of HCFDST specimens illustrating the effect of D_o/t_o.

The outer steel tube thicknesses remain constant while their diameter is changed to study this characteristic. The outer diameter was varied to give Do/to ratios of 75, 90 and 105. When the Do/to ratio of 75 is changed to 90 and 105, the computed ultimate bearing capacity of HCFDS columns is increased by 14.6% and 79.6%, respectively.

4.2. Hollow Ratio Effect (X)

The axial load displacement curves for the different hollow ratio HCFDST specimens are displayed in Fig. 10.

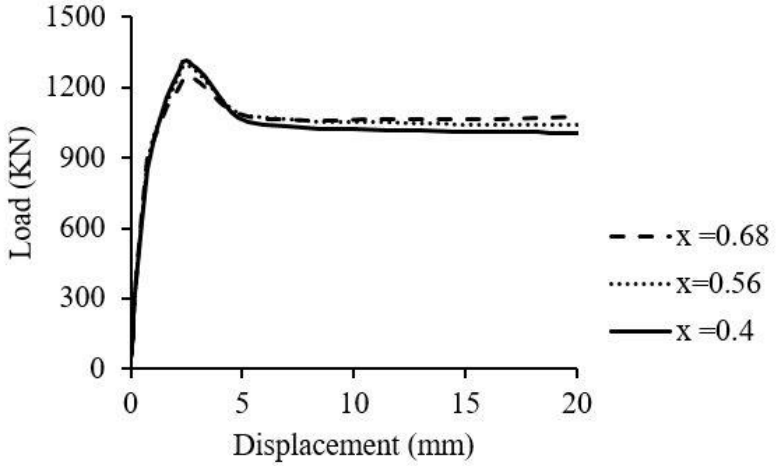

Fig. 10. Load–displacement curves of HCFDST specimens illustrating the hollow ratio effect(χ).

The most important factor affecting the compressive performance of the CFDST columns is the hollow ratio (χ), which can be described as di/(Do-2to). Increasing the hollow ratio (χ) from 0.4 to 0.56 and 0.68 leads to 1.4% and 4.9% decreases in the ultimate bearing capacity, respectively.

4.3. HSC Compressive Strength Effect

The concrete is categorized as high strength concrete (HSC) at 50 MPa < fc ≤ 90 MPa, pursuant to EN 1994-1-1 [27]. The load-displacement curves of HCFDST columns with different fc values are given in Fig. 11.

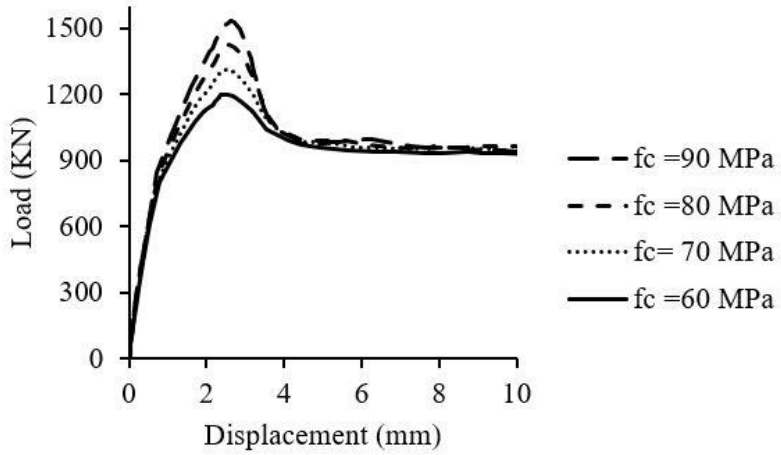

Fig. 11. Load–displacement curves of HCFDST specimens illustrating the concrete f_c value.

When the fc of 60 is changed to 70, 80 and 90 MPa, the ultimate bearing capacity of HCFDST specimens is increased by 9.4%, 18.7% and 27.9%, respectively.

4.4. Effects Of Steel Yield Strengths

Fig. 12 illustrates the load-displacement curves of HCFDST specimens with various yield strengths of steel. The column axial capacity increases by 7.7%, 14% and 26.1%, respectively if the yield strength of steel tubes is modified from 240 to 300, 350, and 450 MPa.

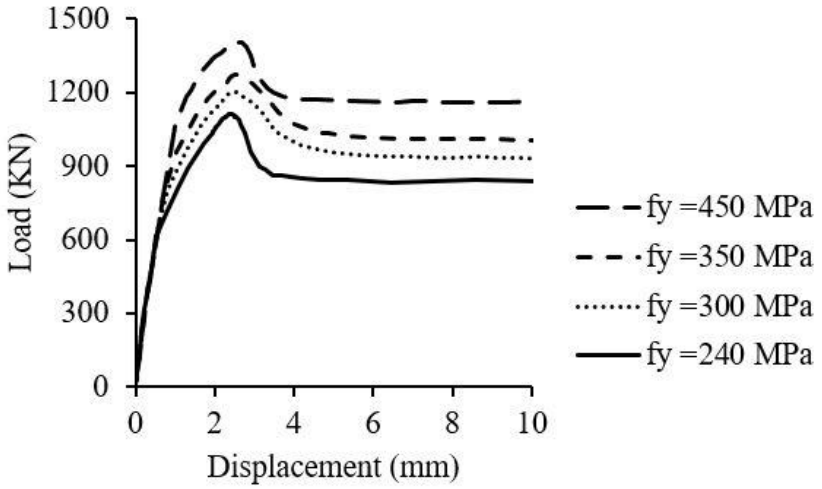

Fig. 12. Load–displacement curves of HCFDST specimens illustrating the steel f_y value.

5. PROPOSED FORMULAE OF BEARING CAPACITY CALCULATION

5.1. Evaluated And Suggested Formulas for Calculating Maximum Bearing Capacity

The ultimate bearing capacity of the HCFDST column can be computed by Eqs. shown below:

$$N_P = f_{scy}A_{sc} + f_{yi}A_{si} \quad (10)$$
$$A_{sc} = A_{so} + A_c \quad (11)$$

Where fscy is the compound axial compressive strength of the sandwich concrete and the outer tube, and Np is the maximum axial capacity. Aso, Asi and Ac are the area of the outer steel tube, inner steel tube, and sandwich concrete, respectively. fyi is the inner steel tubes yield strength. With the aid of the formulas [28], fscy is computed in Eq. (12):

$$f_{scy}/f_c = 1.212 + B\xi + C\xi^2 \quad (12)$$
$$B = m_1 f_y/213 + n_1 \quad (13)$$
$$C = m_2 f_c/14.4 + n_2 \quad (14)$$

Where m1=0.140, n1=0.778, m2= - 0.070 and n2=0.026. ξ, the confinement factor to CFDST [29]:

$$\xi = \frac{A_{so}\, f_{yo}}{A_{ce}\, f_{ck}} \quad (15)$$
$$A_{so} = 6\, b\, t_o \quad (16)$$

Where Aso is the outer steel tube area, b=(B-2to)/$\sqrt{3}$ illustrated in Fig. 3.0 and Ace is the concrete nominal cross-sectional area as shown below:

$$A_{ce} = 1.5\sqrt{3}\, b^2 \quad (17)$$

The following is the equation that used to compute fscy [29]:

$$f_{scy}/f_c = C_1\chi^2 f_{yo}/f_c + C_2(1.14 + 1.02\xi) \quad (18)$$
$$C_1 = \alpha/(1+\alpha) \quad (19)$$
$$C_2 = (1+a_n)/(1+\alpha) \quad (20)$$
$$\alpha = A_{so}/A_c \quad (21)$$
$$a_n = \frac{A_{so}}{A_{ce}} \quad (22)$$

Equations suggested in [19] were presented in [18]. The updated equations are displayed:

$$f_{scy}/f_c = a_o + B\xi + C\xi^2 \quad (23)$$
$$B = a_1(1 + b_1\chi + c_1\chi^2)(1 + df_{yo}/213) \quad (24)$$
$$C = a_2(1 + b_2\chi + c_2\chi^2)(1 + ef_c/14.4) \quad (25)$$

Based on Eqs. (18–20), the modified expression of Eqs. (26-28) is suggested in this study:

$$f_{scy}/f_c = \frac{A_1\chi^2 f_{yo}}{f_c} + A_2(1.14 + 1.02\xi) \quad (26)$$
$$A_1 = b\,(\alpha + c) \quad (27)$$
$$A_2 = b\,[(1 + a_n) + c] \quad (28)$$

Where b and c equal 0.7 and 0.1, respectively.

5.2. Comparisons of FE Results with Different Formulae

The results of various formulae predictions are summarized in Table 3. Table 4 displayed the average and coefficient of variation (COV) of the different formulas. Compared to Eqs. (12), (18), and (23), the COV for Eq. (26) were 0.961 and 0.053, respectively. This demonstrated that the Eq. (26) given in this paper may be used to determine the maximum load capacity of the HCFDST columns.

Table 3: Comparison of F.E. results with the prediction results of various formulas.

Columns	Nul,F.E (kN)	N (12) (kN)	N (18) (kN)	N (23) (kN)	N (26) (kN)	N (12) / Nul,F.E	N (18) / Nul,F.E	N (23) / Nul,F.E	N (26) / Nul,F.E
A150-60-300-60	1201	1217	1238.9	1095	1105	1.013	1.0314	0.911	0.920
A180-60-300-60	1376	1745	1736.3	1513	1499	1.268	1.2616	1.099	1.089
A 210-60-300-60	2157	2356	2312.7	1992	1953	1.093	1.0723	0.924	0.906
A150-50-300-60	1316	1346	1352.4	1200	1189	1.022	1.0273	0.911	0.903
A150-70-300-60	1297	1271	1310.1	1172	1207	0.980	1.0101	0.904	0.931
A150-85-300-60	1252	1178	1248.6	1114	1194	0.941	0.9975	0.890	0.953
A150-60-300-70	1314	1360	1371.1	1203	1214	1.035	1.0434	0.915	0.924
A150-60-300-80	1425	1502	1503.3	1311	1323	1.054	1.0548	0.920	0.928
A150-60-300-90	1536	1645	1635.4	1419	1432	1.071	1.0649	0.924	0.933
A150-60-240-60	1115	1141	1149.7	1007	1015	1.023	1.0313	0.903	0.910
A150-60-350-60	1271	1282	1313.3	1167	1179	1.009	1.0329	0.918	0.928
A150-60-450-60	1406	1417	1461.9	1311	1329	1.008	1.0398	0.932	0.945

Table 4: Mean and COV of the columns.

Indices	N (12) / Nul,F.E	N (18) / Nul,F.E	N (23) / Nul,F.E	N (26) / Nul,F.E
Mean	1.064	1.055	0.953	0.961
COV	0.084	0.065	0.060	0.053

Where mean (x), standard deviation (s) and coefficient of variation (v) are given in Eqs. 29, 30 and 31, respectively according to the ECP203-2020 [30].

$$x = \sum_{i=1}^{n} x_i / n \tag{29}$$

$$s = \sqrt{\frac{1}{n-1}} \sum_{i=1}^{n} (x_i - x)^2 \tag{30}$$

$$v = \frac{s}{x} * 100 \tag{31}$$

6. Conclusions

In this study, the behavior of the double-skinned, composite hexagonal columns filled with concrete (HCFDST columns) was investigated. 12 columns in total were studied to assess and simulate the basic behavior of HCFDST columns under compression. The factors considered in the parametric analysis were the hollow ratio, steel yield stress, outer tube diameter to thickness, and concrete compressive strength. FE models were created and compared to the outcomes of Equations (12), (18), (23) and (26). This allowed for the confirmation of the modeling accuracy. The maximum bearing capacity and load-displacement curves of the test specimens were considered when comparing the test specimens to the specimens represented by the Abaqus model. Overall, the following conclusions can be drawn from the FE results of this investigation:

(1) When the Do/to ratio of 75 is changed to 90 and 105, the maximum bearing capacity of HCFDS column is increased by 14.6% and 79.6%, respectively.

(2) Increasing the hollow ratio (χ) from 0.4 to 0.56 and 0.68 leads to 1.4% and 4.9% decreases in the ultimate bearing capacity, respectively.

(3) When the fc of 60 is changed to 70, 80 and 90 MPa, the ultimate bearing capacity of HCFDST specimens is increased by 9.4%, 18.7% and 27.9%, respectively.

(4) The column axial capacity increases by 7.7%, 14% and 26.1%, respectively if the yield strength of steel tubes is modified from 240 to 300, 350, and 450 MPa.

New formula has been proposed to determine maximum bearing capacity of HCFDST short columns under compression and given by Eq. (26).

7. REFERENCES

[1] Han L-H., Wei L., and Bjorhovde R., "Developments and advanced applications of concrete-filled steel tubular (CFST) structures: members", Journal of Constructional Steel Research, 100, pp 211–228, 2014.

[2] Qing Q.L., "Nonlinear analysis of circular double-skin concrete-filled steel tubular columns under axial compression", Engineering Structures, 131, pp 639–650, 2017.

[3] Yan X-F, Zhao Y-G. "Experimental and numerical studies of circular sandwiched concrete axially loaded CFDST short columns", Engineering Structures, 230, pp 111617, 2021.

[4] Yan X-F, Zhao Y-G. "Compressive strength of axially loaded circular concrete-filled double-skin steel tubular short columns", Journal of Constructional Steel Research, 170, pp 106-114, 2020.

[5] Lu H, Zhao X-L and Han L-H., "Testing of self-consolidating concrete-filled double skin tubular stub columns exposed to fire", Journal of Constructional Steel Research, 66, pp 1069–1080, 2010.

[6] Tao Z, Han L-H and Zhao X-L, "Behavior of concrete-filled double skin (CHS inner and CHS outer) steel tubular stub columns and beam-columns", Journal of Constructional Steel Research, 60, pp1129–1158, 2004.

[7] Uenaka K, Kitoh H and Sonoda K, "Concrete filled double skin circular stub columns under compression", Thin-Walled Structures, 48, pp 19–24, 2010.

[8] Huang H, Han L-H, Tao Z and Zhao X-L. "Analytical behavior of concrete-filled double skin steel tubular (CFDST) stub columns", Journal of Constructional Steel Research, 66, pp 542–555, 2010.

[9] Hassanein MF and Kharoob OF. "Compressive strength of circular concrete-filled double skin tubular short columns", Thin-Walled Struct, 77, pp 165–173, 2014.

[10] Han L-H, Li Y-J, Liao F-Y. "Concrete-filled double skin steel tubular (CFDST) columns subjected to long-term sustained loading", Thin-Walled Structures, 49, pp 1534–1543, 2011.

[11] Sugimoto M., Yokota S., Sonoda K., and Yagishita F., "A basic consideration on double skin tube–concrete composite columns", Osaka City University and Monash University Joint Seminar on Composite Tubular Structures, Osaka, Japan, 1997.

[12] Junchang C., Hong J., Mizan A., Shicai C., Daxing Z., and Liqun H., Experimental and numerical analysis of circular concrete-filled double steel tubular stub columns with inner square hollow section", Engineering Structures, 227, pp 111400, 2021.

[13] Zhao X-L., and Raphael G., "Strength and ductility of concrete filled double skin (SHS inner and SHS outer) tubes", Thin-Walled Structures, 40(2), pp 199-213, 2002.

[14] Elchalakani M., Zhao X-L., and Raphael G., "Tests of concrete filled double skin (CHS outer and SHS inner) composite short columns under axial compression", Thin-Walled Structures, 40(5), pp 415–441, 2002.

[15] Wei S., Mau S., Vipulanandan C., and Mantrala S., "Performance of new sandwich tube under axial loading: analysis", Journal of Structural Engineering, 121(12), pp 1815–1821, 1995.

[16] ABAQUS Standard, User's Manual. The Abaqus software is a product of Dassault Systèmes Simulia Corp., Providence, RI, USA Dassault Systèmes, Version 6.14, USA., 2014.

[17] Elchalakani M., Karrech A., Hassanein M.F. and Yang B., "Plastic and yield slenderness limits for circular concrete filled tubes subjected to static pure bending", Thin-Walled Structures, 109, pp 50-64, 2016.

[18] Dai X. and Lam D., "Numerical modelling of the axial compressive behavior of short concrete-filled elliptical steel columns", Journal of Constructional Steel Research, 66(7), pp 931–942, 2010.

[19] Dai X., Lam D., Jamaluddin N, Ye J., "Numerical analysis of slender elliptical concrete filled columns under axial compression", Thin-Walled Structures, 77, pp 26–35, 2014.

[20] Hassanein M.F., Patel V.I., "Round-ended rectangular concrete-filled steel tubular short columns: FE investigation under axial compression", Journal of Constructional Steel Research, 140, pp 222–236, 2018.

[21] Shen L., Yang B., Ding M., Chen F., Alqawzai S., Elchalakani M. and Chen K., "Experimental study on the behavior of a novel stiffened hexagonal CFDST stub column under axial load", Journal of Structural Engineering, 148(1), 2022.

[22] Yu T, Teng JG, Wong YL and Dong SL. Finite Element Modeling of Confined Concrete-I: Drucker-Prager Type Plasticity Model. Engineering Structure, pp:665–679, 2010.

[23] Mander JB, Priestly MNJ and Park R. Theoretical Stress-Strain Model for confined concrete. Engineering Structure, ASCE, 114(8), pp:1804–1826,1988.

[24] ACI (American Concrete Institute). 2014. Building code requirements for structural concrete and commentary. ACI 318. Chicago: ACI

[25] Liang QQ and Fragomeni S. "Nonlinear Analysis of Circular Concrete-Filled Steel Tubular Short Columns under Axial Loading", Journal of Construction Steel Research, 65 (12), pp:2186–2196, 2009.

[26] Hassanein M.F., Kharoob O.F. and Liang Q.Q., "Circular Concrete-Filled Double Skin Tubular Short Columns with External Stainless Steel Tubes under Axial Compression", Thin-Walled Structures, pp:252–263, 2013.

[27] EN 1994-1-1: Eurocode 2. Design of concrete structures. Part 1–1. General rules and rules for, buildings. European Committee for Standardization, 2004.

[28] MOHURD (Ministry of Housing and Urban-Rural Development of the People's Republic of China). Technical code for concrete filled steel tubular structures. GB 50936-2014. Beijing: MOHURD, 2014.Tao Z., and Han L.-H., "Behavior of Concrete-Filled Double Skin Rectangular Steel Tubular Beam-Columns", Journal of Constructional Steel Research, 62 (7), pp: 631–646, 2006.

[29] Han L-H., Dennis L., and Nethercot D. A., "Design Guide for Concrete Filled Double Skin Steel Tubular Structures", Boca Raton, FL: CRC Press/ Taylor & Francis Group, 2019.

[30] ECP (Egyptian Code for Practice), Egyptian Reinforced Concrete Code. ECP 2